The Astronomical Journal, 168:50 (13pp), 2024 August https://doi.org/10.3847/1538-3881/ad4882

A Study of Nine Extremely Low Mass Ratio-contact Binary Systems

Eleni Lalounta[1], Panagiota-Eleftheria Christopoulou[1], Athanasios Papageorgiou[1], C. E. Ferreira Lopes[2,3,4], and Márcio Catelan[5,6,7]
[1] Department of Physics, University of Patras, 26500, Patra, Greece; pechris@upatras.gr
[2] Instituto de Astronomía y Ciencias Planetarias, Universidad de Atacama, Copayapu 485, Copiapó, Chile
[3] Universidade de São Paulo, IAG, Rua do Matão 1226, Cidade Universitária, São Paulo, 05508-900, Brazil
[4] National Institute For Space Research (INPE/MCTI), Av. dos Astronautas, 1758 - São José dos Campos - SP, 12227-010, Brazil
[5] Instituto de Astrofísica, Pontificia Universidad Católica de Chile, Av. Vicuña Mackenna 4860, 7820436 Macul, Santiago, Chile
[6] Millennium Institute of Astrophysics, Nuncio Monseñor Sotero Sanz 100, Of. 104, Providencia, Santiago, Chile
[7] Centro de Astro-Ingeniería, Pontificia Universidad Católica de Chile, Av. Vicuña Mackenna 4860, 7820436 Macul, Santiago, Chile
Received 2024 April 9; revised 2024 May 2; accepted 2024 May 6; published 2024 July 2

Abstract

Low-mass ratio systems (LMR) are a very interesting class of contact eclipsing binaries challenging the theoretical models of stability. These systems are also considered possible progenitors of the rare low-mass optical transients called red novae. In this study, we present the identification of 7 new totally eclipsing LMR systems from Catalina Sky Surveys (CSS) and 77 LMR candidates from the All Sky Automated Survey. Using the available CSS light curves and new multiband observations for CSS_J210228.3-031048 and CSS_J231513.3+345335 with the 2.3 m Aristarchos telescope at Helmos Observatory, we estimate their physical and absolute parameters and investigate their stability and their progenitors. The light curves are analyzed by performing a two-dimensional scan on the mass–ratio inclination plane with Phoebe-0.31 scripter, while the errors are estimated using Monte Carlo simulations and heuristic scanning of the parameter space. Our analysis revealed that all 9 CSS systems have extreme mass ratios from 0.09 to 0.16. Our statistical analysis of well-studied LMR contact binaries shows that LMR systems tend to have warmer and more massive primaries. The investigation of the progenitors of both low and higher-mass-ratio systems reveals a trend for the former to originate from higher-mass ancestors. Finally, we investigate the stability condition by calculating the ratio of spin angular momentum to orbital angular momentum and other stability indicators in the context of the reliability of the solutions.

Unified Astronomy Thesaurus concepts: Surveys (1671); Interacting binary stars (801); Eclipsing binary stars (444); Stellar evolution (1599); Contact binary stars (297); Fundamental parameters of stars (555)

1. Introduction

The discovery of a plethora of binaries in the era of large surveys, the availability of advanced follow-up facilities, and the analysis of observations with sophisticated modeling tools have recently led to a resurgence in the study of the origin, structure, and evolution of binary systems.

Contact binaries (also called EW or W UMa systems) are composed of two Roche-lobe-filling, strongly interacting stars, usually of a late type, that share a common envelope. Detached cool binaries with an initial period of a few days that lose mass and angular momentum through magnetic braking are thought to be their progenitors. The time evolution of the orbital period and observed mass ratio of EWs are governed by the interplay between mass transfer/loss processes, angular momentum loss (AML), tidal effects, and the presence of additional components. How contact binaries of low/moderate mass end their lives catastrophically by merging into a single star or going through "common envelope" events is still debated. Although theoretical models of an EW containing two main sequence stars predict coalescence due to the tidal Darwin instability (e.g., Darwin 1879; Hut 1980) at a minimum secondary-to-primary mass ratio ($q_{\rm min}$) below 0.07–0.1 (Rasio 1995; Arbutina 2009), many new EWs beyond this limit have been discovered photometrically (Christopoulou et al. 2022 and references therein) by Kepler and ground-based wide-field surveys, including the Robotic Optical Transient Search Experiment (Akerlof et al. 2000), All Sky Automated Survey (ASAS-3; Pojmanski 1997, 2002), Super Wide Angle Search for Planets (Butters et al. 2010), Catalina Sky Surveys (CSS; Drake et al. 2009, 2014a), Asteroid Terrestrial-impact Last Alert System (Heinze et al. 2018), and Zwicky Transient Facility (ZTF; Bellm et al. 2019). This notwithstanding, there is only one documented merging event in the Milky Way, V1309 Sco (Tylenda et al. 2011), which became the prototype of a new class of low-mass optical transients known as red novae. According to observational preoutburst constraints and retrieved from archival data, many researchers (Stępień 2011; Nandez et al. 2014) have shown that V1309 Sco's progenitor was an eclipsing contact binary with a period of 1.4 days and an extremely low mass ratio, composed of an early subgiant and a low-mass companion. Kochanek et al. (2014) estimated that Galactic stellar mergers such as V1309 Sco occur once per decade. Therefore, the identification of candidate systems before the merger event among low-mass-ratio (LMR) contact systems is of great importance for the understanding of the mechanisms involved.

The suitability of survey data for light-curve analysis has not been thoroughly examined. According to Sun et al. (2020), there was good agreement between ASAS-SN photometric data in comparison to ground-based observations regarding the mass ratio. This was also confirmed by Christopoulou et al. (2022) between CSS and dedicated data. Devarapalli et al. (2020), Zheng et al. (2021), and Wadhwa et al. (2022) showed the

Table 1
Basic Information for the 9 LMR EW Systems from CSS

ID	Short ID	R.A.$_{J2000}$ (h:m:s)	Decl.$_{J2000}$ (°:′:″)	HJD$_0$ (2450000+)	Period (days)	V_{CSS}(max) (mag)	σ_{CSS} (mag)	N_p
CSS _ J014859.6+391504	J014859	01:48:59.65	+39:15:04.2	5479.72138	0.7777702	14.86	0.02	271
CSS _ J065207.9+530125	J065207	06:52:07.92	+53:01:25.6	5093.00000	0.7608190	13.53	0.01	293
CSS _ J090748.9+375447	J090748	09:07:48.94	+37:54:47.3	6404.69949	0.3092479	13.31	0.01	380
CSS _ J101256.9+313709	J101256	10:12:56.97	+31:37:09.6	4096.81447	0.3627181	13.86	0.01	408
CSS _ J153254.1+342518	J153254	15:32:54.17	+34:25:18.1	4157.85294	0.4550895	13.71	0.01	286
CSS _ J174213.4+440857	J174213	17:42:13.49	+44:08:57.3	3507.86169	0.4245780	14.14	0.02	286
CSS _ J210228.3-031048	J210228	21:02:28.30	−03:10:46.9	6208.99231	0.2454814	14.40	0.02	421
CSS _ J224702.1+362815	J224702	22:47:02.10	+36:28:15.8	4953.96243	0.4849898	14.82	0.02	212
CSS _ J231513.3+345335	J231513	23:15:13.35	+34:53:35.9	5985.73362	0.2661317	15.06	0.02	315

same agreement on the mass ratio and fractional radii, with some variations in the fill-out factor and temperature ratio.

As part of an ongoing project to find LMRs in CSS data, we present the identification and photometric investigation of seven new totally eclipsing LMRs found in CSS. Additionally, we conduct multiband photometry and analysis for two totally eclipsing LMRs (Lalounta et al. 2020) included also in the automatic photometric analysis of Sun et al. (2020) of 2335 late-type contact binaries from CSS.

The 9 systems were first classified as EW type by Drake et al. (2014b). Later, Lalounta et al. (2020) included these systems in a sample of 2101 LMR candidates showing total eclipses found in CSS, applying Fourier decomposition on the phase-folded and normalized flux light curves (LCs). Recently, Christopoulou et al. (2022) presented the identification and photometric analysis of the first 30 new LMRs from the above sample (see the paper for details of the methodology employed).

The paper is organized as follows: in Section 2, we present all the information about the observations of the objects together with CSS data. In Section 3, we describe the photometric analysis of the light curves, and the physical and absolute parameters determination with their errors. Finally, in Section 4 we discuss our results and investigate the possibility of our sources being merger candidates. New possible LMRs from ASAS-3 are also presented in the Appendix.

2. CSS and New Photometric Observations

In this study, we use the photometric data obtained from the Catalina Real-Time Transient Survey Data Release 2 (Drake et al. 2014b), which covers 9 yr (2004–2013). The observations are taken unfiltered to maximize the throughput and then the magnitudes are transformed to an approximate V magnitude (Drake et al. 2013). The nine studied systems have sufficiently sampled LCs with more than 200 observations (N_p). Table 1 provides the basic information of the 9 LMR EWs, such as the coordinates (R.A.$_{J2000}$ and decl.$_{J2000}$), the reference time of minimum (in Heliocentric Julian Days; HJD$_0$), Period (in days), the CSS magnitude at maximum light (V_{CSS}(max)), the mean photometric error (σ_{CSS}; calculated according to the analytical expression derived by Papageorgiou et al. 2018; their footnote 8), and the number of available CSS observations (N_p).

In addition, follow-up multicolor observations were carried out for the two shortest period of the nine systems, J210228 (0.2455 day) and J231513 (0.2661 day), using the Aristarchos telescope at Helmos Observatory, Greece. This 2.3 m Ritchey-Chrétien telescope is equipped with a liquid nitrogen-cooled VersArray 1024B CCD camera with 1024 × 1024 pixels and a standard *BVRI* filter set. The pixel scale is 0.″28, which gives an effective field of view of 4.′8 × 4.′8. Image reduction and differential photometry were performed using a fully automated pipeline (Papageorgiou & Christopoulou 2015a) that incorporates Pyraf (Science Software Branch at STScI 2012) and the Astrometry.net packages (Lang et al. 2010).

J210228 was observed on five nights in total, three in 2019 (August 9–11 and 21), and two in 2021 (September 14 and 15). 2MASS J21023075-0313205 (Johnson *V*-band magnitude $V_J = 14.8$ mag) was used as comparison star, 2MASS J21023485-0309335 ($V_J = 15.7$ mag) as check star, and the photometric precision is estimated as 0.024–0.050 mag, 0.007–0.020 mag, 0.008–0.010 mag, and 0.009–0.020 mag in *BVRI*, respectively, depending on the observing conditions.

J231513 was observed on three nights in total (2019 September 21 2020 October 11, and 2021 September 14). 2MASS J23151130+3455434 ($V_J = 15.5$ mag) was used as comparison star, 2MASS J23145819+3454092 ($V_J = 15.5$ mag) as check star, and the photometric precision is estimated as 0.008–0.012 mag, 0.006–0.008 mag, and 0.007–0.010 mag in *VRI*, respectively, depending on the observing conditions.

3. Light-curve Modeling

All nine systems show total eclipses (Figure 1). Totality, in the case of EWs, gives a reliable determination of the photometric mass ratio,[8] q (Terrell & Wilson 2005; Hambálek & Pribulla 2013; Şenavcı et al. 2016) when radial velocities are not available. Thus, the CSS and the new multiband LCs were analyzed using the PHOEBE-0.31a scripter (Prša & Zwitter 2005) in "Overcontact not in thermal contact" mode. Since the LC morphology constrains only the temperature ratio (T_2/T_1) of the two components, an estimation of the primary's effective temperature T_1 is needed. We adopt the effective temperatures of the systems (T_{sys}) from Stassun et al. (2019), and assuming that the T_{sys} is dominated by the temperature of the hotter component (T_1), we set $T_1 = T_{sys}$ as a fixed value. For J065207, J090748, and J101256 the adopted spectroscopic value of effective temperature is in agreement with the Large Sky Area Multi-Object Fiber Spectroscopic Telescope (LAMOST) low-resolution spectrum (Cui et al. 2012) data (Qian et al. 2020), and for J174213 from LAMOST observations (1 May 2017) within errors. For J014859, J210228, J224702, and J231513 there are no spectroscopic data whereas

[8] Where $q = M_2/M_1$. In this work, we denote with index 1 the parameters of the more massive (primary) and 2 those of the less massive (secondary) component.

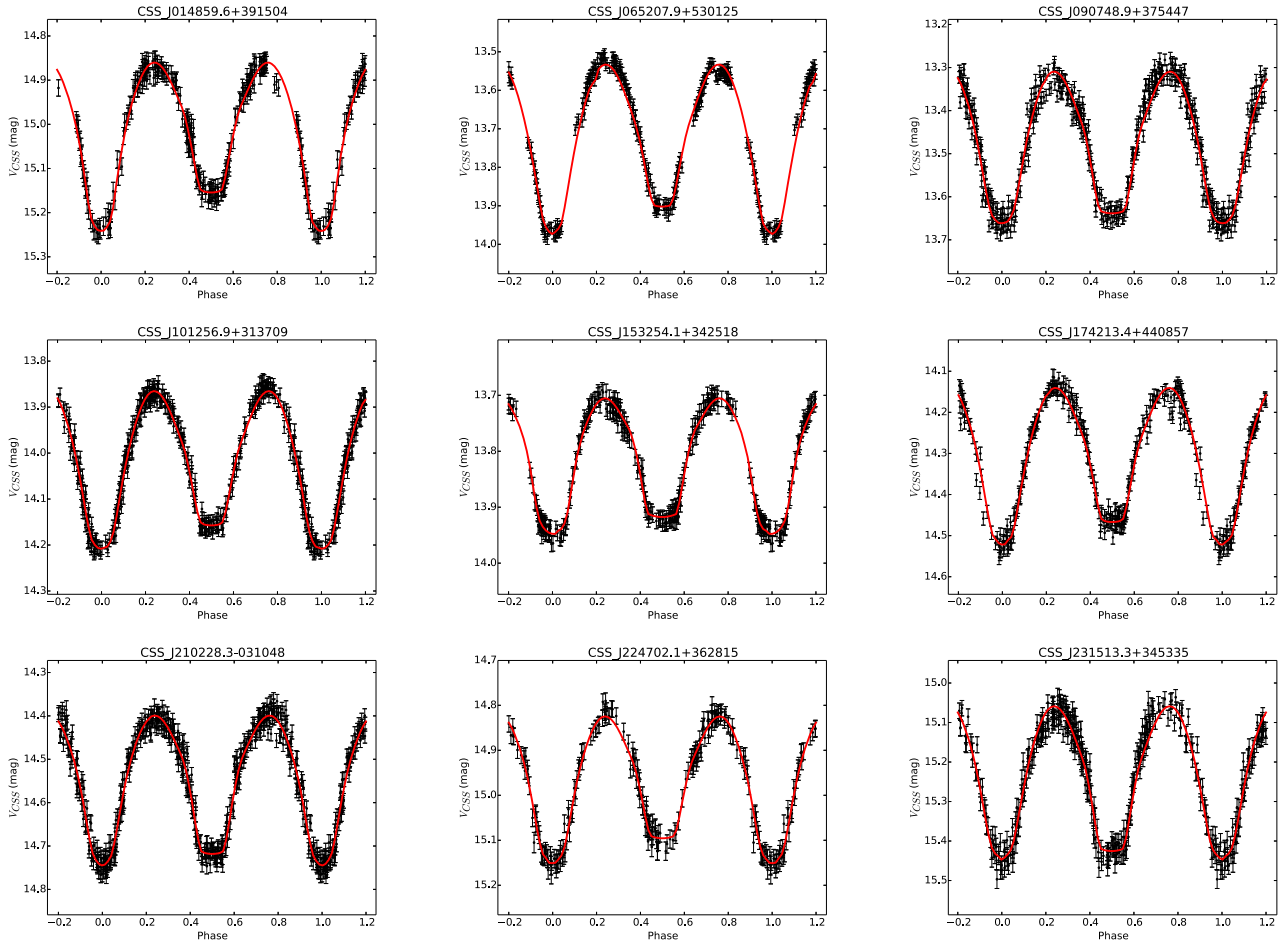

Figure 1. The observed LCs (black points) from CSS and the best-fitted models (red lines) for the nine LMR systems.

for J153254 we set the effective temperature 6747 ± 45 K from LAMOST (9 March 2015). The limb-darkening coefficients were interpolated from van Hamme (1993) tables for the given temperatures, while the bolometric albedos and the gravity darkening coefficients were set as $A_1 = A_2 = 0.5$ (Ruciński 1973) and $g_1 = g_2 = 0.32$ (Lucy 1967), respectively, for $T_{\rm sys} < 7200$ K and $A_1 = A_2 = 1$ and $g_1 = g_2 = 1$ otherwise. The synchronicity parameter was set as $F_{1,2} = 1$, which corresponds to a synchronous rotation, in a circular orbit. Finally, the ephemeris of each system was improved by adjusting the period and the reference time of minimum, $\rm HJD_0$ (see Table 1).

Our next step was to perform a 2D grid search on the mass–ratio inclination ($q - i$) plane in order to determine the pair ($q_{\rm min}$, $i_{\rm min}$) that minimizes the χ^2 of the observed minus calculated LC. In a first attempt to estimate ($q_{\rm min}$, $i_{\rm min}$), the range of q was set at [0.1–0.6], with an increment of 0.05, and the range of i at [65°–90°], with an increment of 1°. This was executed into two runs, one with phase shift 0.0 and a second with 0.5 to investigate values of $q \leqslant 1$ and $q > 1$, respectively. Then, depending on the first results, the explored q values were set in the range of $q_{\rm min} \pm 0.05$, with an increment of 0.01. The derived physical parameters from the fitting, namely mass ratio q, temperature ratio T_2/T_1, modified equipotential $\Omega_{1,2}$, relative radii of the components $r_{1,2}$, inclination i, bandpass luminosity of the primary component over the total bandpass luminosity $L_1/L_{\rm tot}$, and fill-out factor[9] f, are listed in Table 2. The third light contribution was also investigated and found to be negligible ($\leqslant$1%) given the photometric precision of CSS LCs.

We chose to model the new multiband LCs of J210228 and J231513 independently from that of CSS to investigate whether the two solutions agree. The results are also presented in Table 2 and show that the modified equipotential $\Omega_{1,2}$, and subsequently the fill-out factor f, as well as the temperature ratio T_2/T_1, are mainly affected, while the mass ratio q and the inclination i is the same within the errors (see Section 3.1). This was also pointed out by Liu et al. (2023), Wadhwa et al. (2023), and Liu et al. (2024). Figure 2 presents the observed LCs and the best-fitted model (black line). As one can clearly see from Figure 2, the dedicated multiband observations reveal an asymmetry at the maxima of both J210228 and J231513, suggestive of the O'Connell effect (O'Connell 1951) possibly caused by chromospheric spots on the surface of the components or one hot spot due to the mass transfer. In the case of J210228, two spots were needed to describe the observed LCs: a hot one on the primary component (colatitude 100° and longitude 15°) and a cool one on the secondary (colatitude 100° and longitude 15°). The hot spot has a radius of 20° and a temperature factor of $T_{\rm s}/T_1 = 1.05$ (where $T_{\rm s}$ is the

[9] $f = \frac{\Omega - \Omega_{\rm in}}{\Omega_{\rm out} - \Omega_{\rm in}}$, where $\Omega_{\rm in}$ and $\Omega_{\rm out}$ are the modified potential at the inner (L_1) and the outer (L_2) Lagrangian points, respectively.

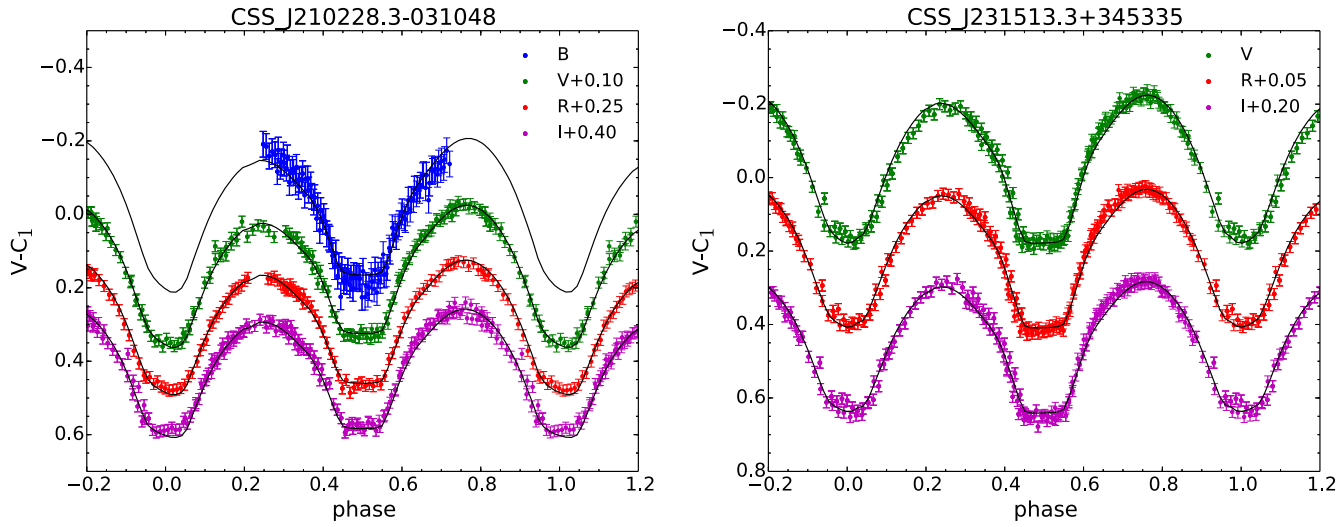

Figure 2. Phase-folded *BVRI* (left) and *VRI* (right) observations for J210228 and J231513, respectively, with their models (black line).

Table 2
The Physical Parameters of the Nine LMR EW Systems from CSS. The second lines for CSS _ J210228.3-031048 and CSS _ J231513.3+345335 Show the Resulting Physical Parameters from the New Multiband LCs

ID	q	$\frac{T_2}{T_1}$	$\Omega_{1,2}$	r_1	r_2	$i(^\circ)$	$\frac{L_1}{L_{\rm tot}}$	f
CSS _ J014859.6+391504	0.16 ± 0.02	0.940 ± 0.012	2.085 ± 0.009	0.558 ± 0.037	0.254 ± 0.044	82.9 ± 2.8	0.865	0.43 ± 0.09
CSS _ J065207.9+530125	0.16 ± 0.02	0.983 ± 0.011	2.029 ± 0.003	0.583 ± 0.012	0.285 ± 0.017	79.2 ± 1.6	0.824	0.98 ± 0.03
CSS _ J090748.9+375447	0.10 ± 0.02	1.046 ± 0.013	1.897 ± 0.004	0.610 ± 0.021	0.244 ± 0.030	79.6 ± 3.1	0.843	0.96 ± 0.07
CSS _ J101256.9+313709	0.11 ± 0.02	0.993 ± 0.008	1.925 ± 0.002	0.602 ± 0.008	0.248 ± 0.011	77.3 ± 1.3	0.865	0.91 ± 0.02
CSS _ J153254.1+342518	0.09 ± 0.02	0.986 ± 0.011	1.922 ± 0.011	0.591 ± 0.048	0.202 ± 0.060	83.6 ± 2.6	0.900	0.09 ± 0.18
CSS _ J174213.4+440857	0.14 ± 0.02	0.987 ± 0.008	2.006 ± 0.006	0.581 ± 0.025	0.260 ± 0.031	80.5 ± 2.4	0.847	0.77 ± 0.07
CSS _ J210228.3-031048	0.13 ± 0.02	1.017 ± 0.007	2.021 ± 0.011	0.569 ± 0.045	0.234 ± 0.054	79.9 ± 5.4	0.848	0.31 ± 0.13
	0.15 ± 0.01	1.011 ± 0.001	2.030 ± 0.002	0.574 ± 0.010	0.259 ± 0.011	79.4 ± 4.0	0.830[a]	0.57 ± 0.03
CSS _ J224702.1+362815	0.11 ± 0.02	0.981 ± 0.016	1.945 ± 0.008	0.593 ± 0.035	0.236 ± 0.043	80.2 ± 2.2	0.878	0.62 ± 0.11
CSS _ J231513.3+345335	0.12 ± 0.02	1.044 ± 0.010	1.953 ± 0.012	0.594 ± 0.055	0.251 ± 0.071	79.7 ± 4.3	0.826	0.84 ± 0.16
	0.14 ± 0.02	1.056 ± 0.001	2.011 ± 0.002	0.579 ± 0.002	0.258 ± 0.002	80.2 ± 3.0	0.802[b]	0.71 ± 0.03

Notes.
[a] In V_J band. The $L_1/L_{\rm tot}$ in BRI bands are 0.827, 0.832, and 0.833, respectively.
[b] In V_J band. The $L_1/L_{\rm tot}$ in RI bands are 0.810, and 0.810, respectively.

temperature on the spot surface) while the cool spot has a radius of 30° and a temperature factor of $T_s/T_2 = 0.75$.

In the case of J231513, one cool spot ($T_s/T_1 = 0.96$), with a radius of 20° on the primary (colatitude 90° and longitude 270°) can satisfactorily describe the observed LCs.

3.1. Error Estimation of the Physical Parameters

The errors provided in Table 2 were estimated using Monte Carlo simulations (Papageorgiou & Christopoulou 2015b; Papageorgiou et al. 2019). During this procedure, 1000 synthetic LCs are produced from the observed ones by a random displacement of each photometric point. The displacement depends on the photometric error ($\sigma_{\rm CSS}$) of the corresponding point (a value selected randomly from a normal distribution with zero mean and $\sigma_{\rm CSS}$ as standard deviation). Finally, the errors are extracted from each parameter's (T_2/T_1, $\Omega_{1,2}$, r_1, r_2, i) distribution within 3σ.

In the case of the new multiband observations of J210228 and J231513, the errors were estimated using parameter kicking (Prša & Zwitter 2005; Papageorgiou 2015) with the PHOEBE-0.31a scripter. This procedure achieves the same effect as stochastic methods (e.g., simulated annealing) but in a significantly shorter time (Prša 2018). Starting from the solution derived by the $q-i$ scan, the parameters T_2/T_1, $\Omega_{1,2}$, i, L_1 are adjusted (80 iterations) and then perturbed by a factor of 5% of their value. The updated model is used as the initial one in order to start a second run, and the loop is repeated 100 times. The errors of the parameters (T_2/T_1, $\Omega_{1,2}$, r_1, r_2, i) are estimated from their distribution within 3 σ. In this way, it is possible to escape the local minima and test the stability of the solution. Nevertheless, the errors of some physical parameters, particularly the fill-out factor f, are underestimated. This may result, as mentioned earlier, from the difference in photometric accuracy between survey and dedicated data or among different surveys. The mass-ratio uncertainties δq were estimated from the $q-i$ scan following the method described by Christopoulou et al. (2022). Figures 3 and 4 present the log χ^2 topology on the $q - \sin i$ plane derived from the $q-i$ scan. The white cross shows the solution along with its errors derived from heuristic scanning.

3.2. Absolute Parameters Estimation

Having determined the temperature (T_2/T_1) and the radii (r_2/r_1) ratio of the systems' components, we use the relation of

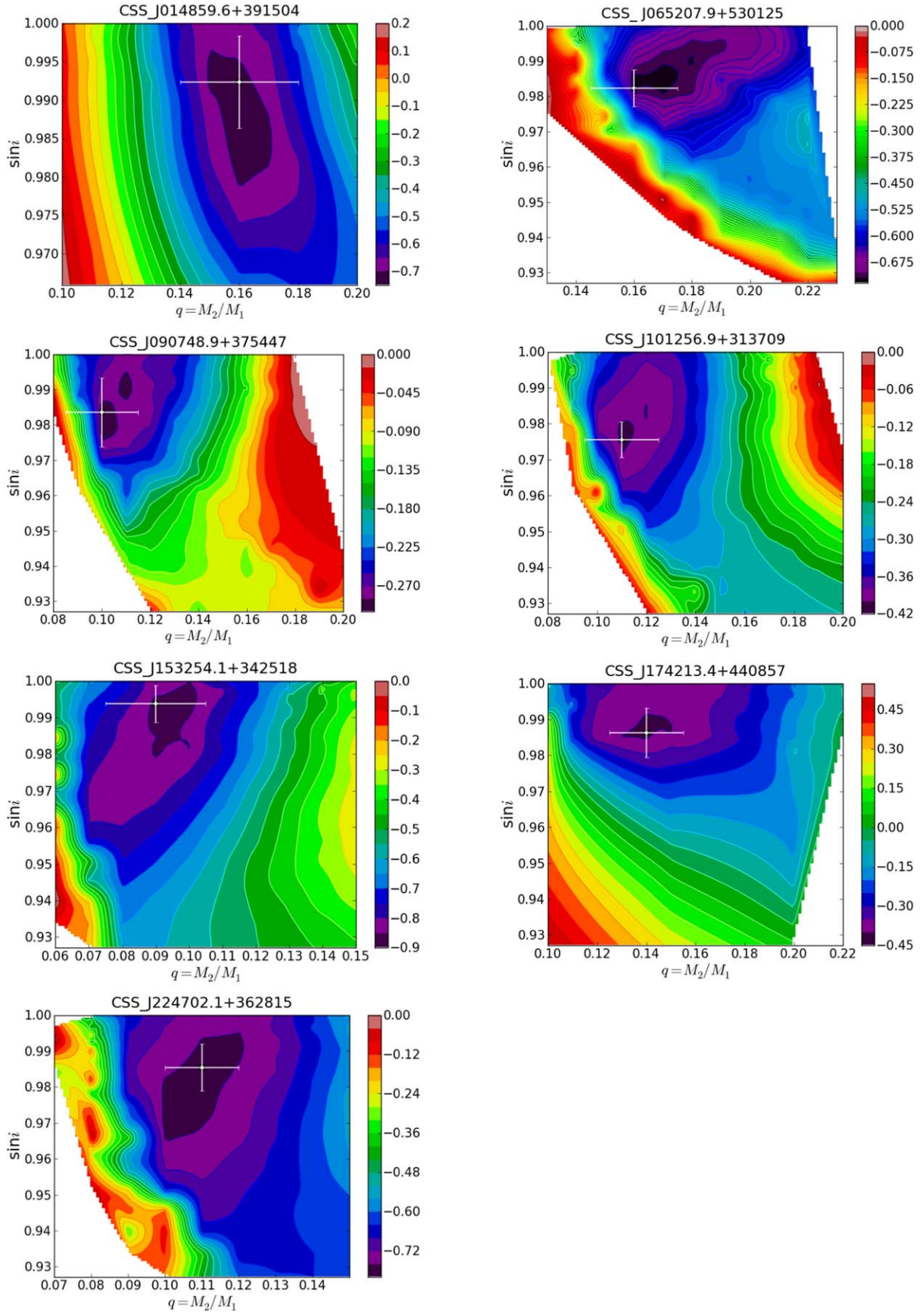

Figure 3. Contour plots of $\log \chi^2$ (color coded according to the scale on the right) on the $(q, \sin i)$ plane as resulted from the $q - i$ scan using the CSS LC. The white crosses represent the solutions of the systems with the error bars derived from the MC and heuristic scanning, respectively. The size of the error bars is drawn according to the errors.

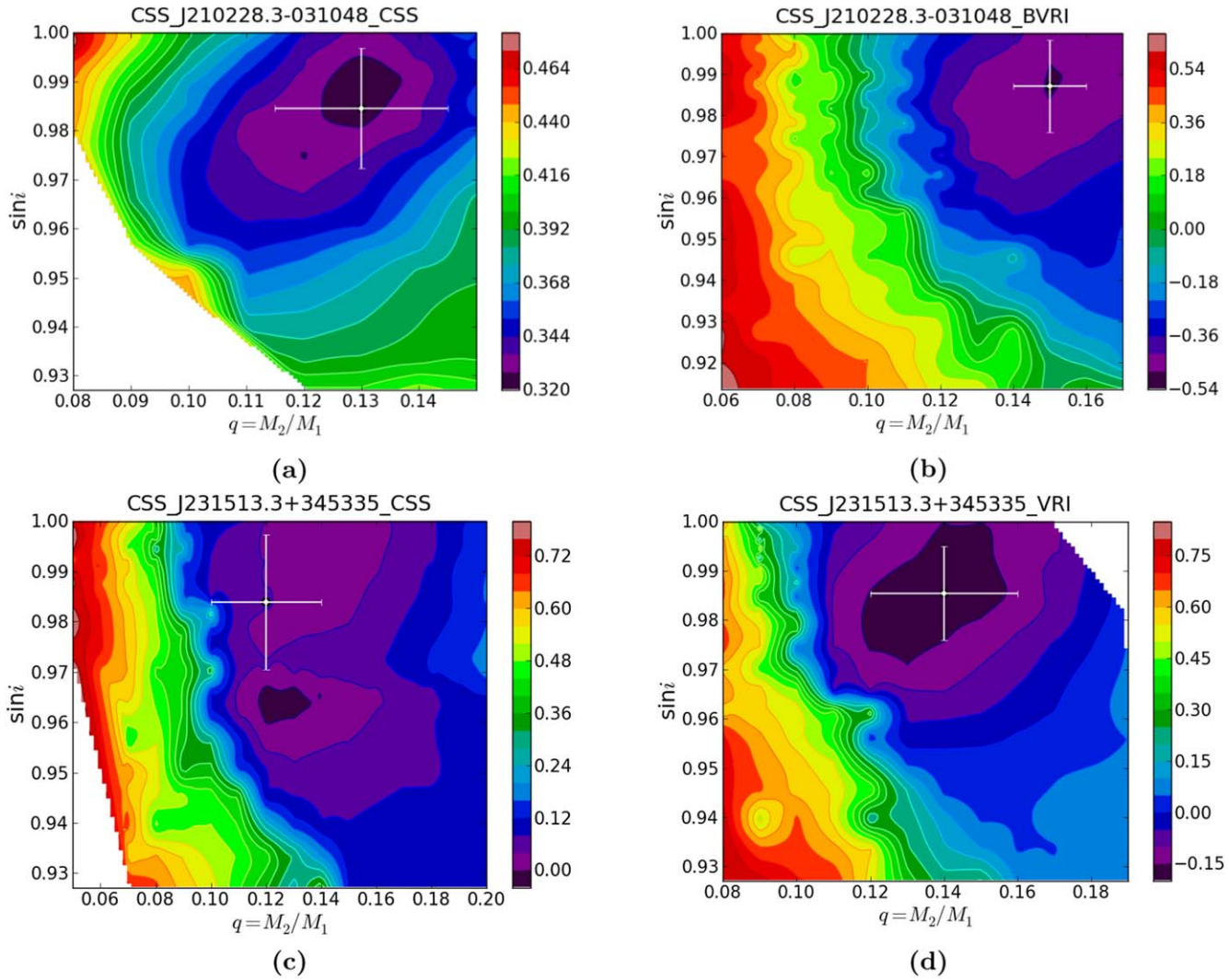

Figure 4. Same as Figure 3 but for J210228 (upper panel) and J231513 (lower panel) using CSS (left) and new *BVRI* observations (right).

Zwitter et al. (2003) to derive the individual effective temperatures T_1, T_2 (Table 3). Then, in order to estimate the absolute parameters of the nine systems, we use our semiempirical mass–luminosity relation for the primary component (Christopoulou et al. 2022; Papageorgiou et al. 2023), namely:

$$\log L_1 = \log(0.63 \pm 0.04) + (4.8 \pm 0.2)\log M_1. \quad (1)$$

This relation is derived using a sample of 161 spectroscopically studied EWs with well-determined absolute parameters, by performing a linear fitting on the $\log M_1 - \log L_1$ plane (see Papageorgiou et al. 2023). We estimate the luminosity of the primary component L_1 using the magnitude at the maxima of the LCs (Table 1) and the luminosity ratio $L_1/L_{\rm tot}$ (Table 2) as derived from the modeling, taking advantage of the new distances from Gaia Data Release 3 (Gaia Collaboration et al. 2023). All the nine systems have well-determined distances with uncertainties $\lesssim$6% of their value, except J014859 (15%). The CSS magnitudes were transformed to *V* Johnson according to the relation from Drake et al. (2013) using *B-V* color indices from TESS Input Catalog, v-8.0 (Stassun et al. 2019). The color extinction A_V was adopted from MWDUST (Bovy et al. 2016; Green et al. 2019) for the given distances, while the required bolometric corrections are obtained from (Pecaut & Mamajek 2013, version 2022.04.16) for the given temperature of the primary. Following the determination of the mass of the primary (M_1), the mass of the secondary M_2 is calculated using the mass ratio q, while the radii (R_1, R_2) of the components are derived using Kepler's law and the relative radii obtained from modeling (Table 2). The results of this procedure are summarized in Table 3, along with the errors in the derived parameters, derived using error propagation. We use the solutions obtained from our data for the absolute parameters estimation of J210228 and J231513.

4. Discussion and Conclusions

We present the identification and photometric investigation of seven new LMR totally eclipsing contact binaries discovered in the CSS as well as multiband photometry and analysis of two totally eclipsing LMRs included in the automatic photometric analysis by Sun et al. (2020) of 2335 late-type contact binaries from CSS. All seven were found to be of extremely low mass ratio, ranging from 0.09 to 0.16.

Table 3
The Absolute Parameters of the Nine LMR EW Systems from CSS

ID	T_{sys} (K)	T_1 (K)	T_2 (K)	M_1 ($M_\odot$)	M_2 ($M_\odot$)	R_1 ($R_\odot$)	R_2 ($R_\odot$)	L_1 ($L_\odot$)	L_2 ($L_\odot$)
CSS _ J014859.6+391504	7045 ± 271	7113 ± 274	6686 ± 257	2.06 ± 0.15	0.33 ± 0.05	2.66 ± 0.19	1.21 ± 0.21	20.38 ± 6.62	2.62 ± 1.00
CSS _ J065207.9+530125	7262 ± 63	7286 ± 63	7162 ± 62	1.73 ± 0.05	0.28 ± 0.04	2.58 ± 0.06	1.26 ± 0.08	8.72 ± 0.61	3.74 ± 0.47
CSS _ J090748.9+375447	5625 ± 112	5588 ± 111	5845 ± 116	1.11 ± 0.03	0.11 ± 0.02	1.25 ± 0.05	0.50 ± 0.06	1.04 ± 0.13	0.26 ± 0.07
CSS _ J101256.9+313709	6295 ± 76	6301 ± 76	6257 ± 75	1.38 ± 0.03	0.15 ± 0.03	1.49 ± 0.03	0.61 ± 0.03	3.03 ± 0.20	0.52 ± 0.05
CSS _ J153254.1+342518	6747 ± 45	6757 ± 45	6662 ± 44	1.67 ± 0.05	0.15 ± 0.03	1.80 ± 0.15	0.61 ± 0.18	7.46 ± 0.37	0.67 ± 0.40
CSS _ J174213.4+440857	6331 ± 178	6345 ± 178	6262 ± 176	1.50 ± 0.04	0.21 ± 0.03	1.65 ± 0.07	0.74 ± 0.09	4.45 ± 0.31	0.75 ± 0.20
CSS _ J210228.3-031048	6140 ± 209	6129 ± 209	6195 ± 211	1.16 ± 0.03	0.17 ± 0.01	1.04 ± 0.02	0.47 ± 0.02	1.28 ± 0.16	0.29 ± 0.05
CSS _ J224702.1+362815	6333 ± 142	6349 ± 142	6228 ± 140	1.55 ± 0.05	0.17 ± 0.03	1.85 ± 0.11	0.74 ± 0.14	5.24 ± 0.67	0.73 ± 0.28
CSS _ J231513.3+345335	5548 ± 145	5493 ± 144	5803 ± 152	1.02 ± 0.04	0.14 ± 0.01	1.06 ± 0.01	0.47 ± 0.01	0.71 ± 0.13	0.23 ± 0.02

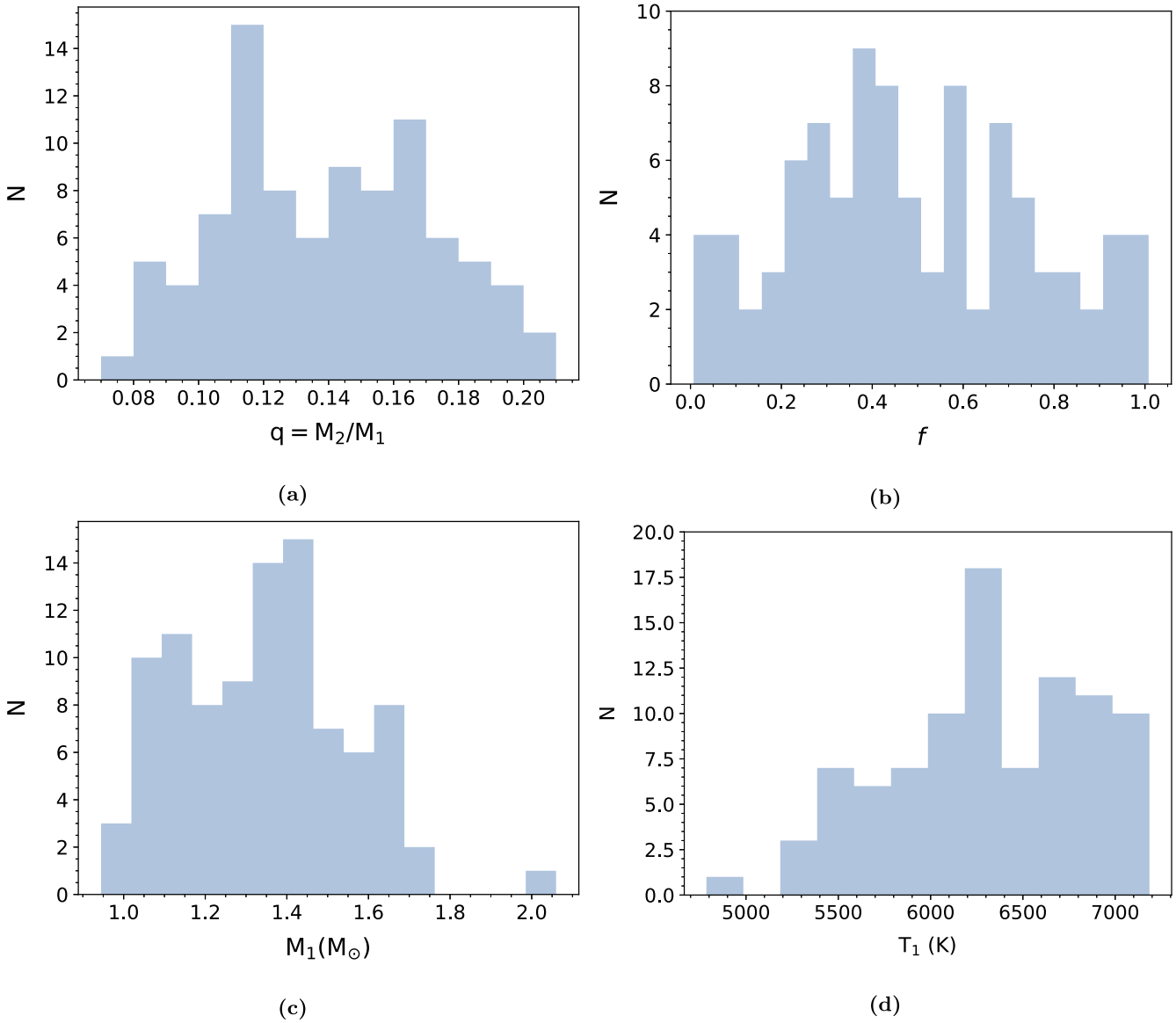

Figure 5. The distributions of (a) q, (b) f, (c) M_1, and (d) T_1 of the 92 CSS LMRs.

In our first application of the Fourier LMR discovery project to the CSS survey, we identified 92 systems (Lalounta et al. 2020). Among these, 37 systems were previously unknown (Christopoulou et al. 2022; our current work), while the remaining 55 were previously reported by Sun et al. (2020). For our analysis, we focused on the sample of 92 LMRs, ensuring consistency in methodology and assumptions to perform limited statistics. As shown in Figure 5, the mass ratio distribution of the 92 CSS LMR systems has a peak at 0.12, although a significant number of systems has $q = 0.17$. In 10% of the systems, q is less than 0.10, with the lowest recorded value being 0.07 ± 0.02 (J075839). The primary masses M_1 are in the range of $1.0 - 1.4\,M_{\odot}$, whereas there are many systems with $M_1 > 1.4\,M_{\odot}$, which is unusual for EW systems (e.g., 22% of EW systems have $M_1 > 1.5\,M_{\odot}$). The distribution of T_1 shows that the majority has $T_1 > 6000\,K$, and 13% have $T_1 > 7000\,K$, which is unusual given the common range of 5500–6000 K of EW systems (Latković et al. 2021). Half of the 92 LMRs have $f > 45\%$ and within the uncertainties of the fill-out parameter, belong to deep contact systems. Figure 6(a) shows a histogram of the period distribution for our sample of 92 CSS LMRs and the 98 new LMR candidates from ASAS-3 (see the Appendix). 20% of systems have $P > 0.5$ day.

To compare the 92 LMRs with the rest of the EWs, we also included 173 well-studied (q from spectroscopy or/and total eclipses) LMRs from the literature from the catalog of Christopoulou et al. (2022), updated up to 2023 with ∼50 more systems (total 317 LMRs) with $0.05 < q < 0.25$, and the 253 well-studied EWs from Latković et al. (2021) with $q > 0.25$ (so as not to overlap with the LMRs). The dependence of T_1 on q, M_1, and $M_{\rm tot}$ for the two samples is presented in Figure 6(b), (c), and (d), respectively. The histogram on the upper panel in each plot represents the distribution of T_1 for each sample, whereas the right-hand histograms in (c) and (d) represent the distribution of M_1 and $M_{\rm tot}$, respectively, for the two samples. Note that the histogram of T_1 in Figure 6(b) is slightly different from that of Figure 6(c) and (d), as no absolute parameters have been determined for all LMRs and EWs. As displayed in Figure 6(c), LMR systems show a trend to have warmer (top histogram) and more massive (right histogram) primaries.

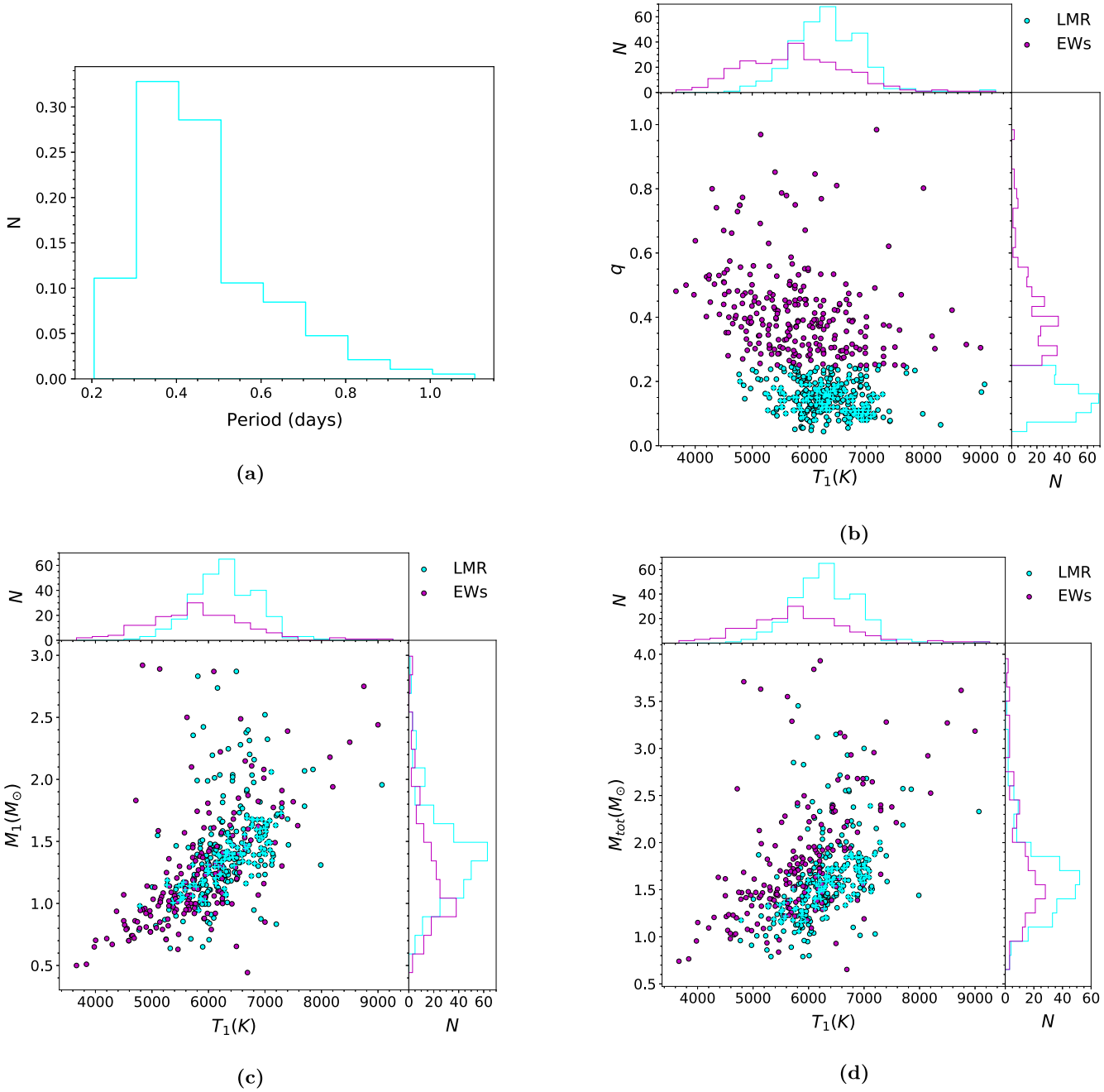

Figure 6. (a) The period distribution of the 92 LMRs from CSS and the 98 LMRs from ASAS-3. (b–d) Dependence of T_1 on q, M_1, and $M_{\rm tot}$ respectively, for the sample of 317 LMRs (cyan) and the 253 well-studied EWs (Latković & Čeki 2021; purple). The upper panel in each plot represents the corresponding distributions of T_1 for the two samples whereas the right-hand histograms in (c) and (d) represent the distribution of M_1 and $M_{\rm tot}$, respectively, for the two samples.

To further investigate the properties of the LMRs, we calculated the mean densities of the primary and secondary components, $\rho_{1,2}$ for both the 92 CSS and the literature systems (from Latković et al. 2021). The results show that systems with shorter periods tend to consist of components with larger ρ_1, while for periods shorter than 0.4 days, systems with the same period have a higher f for smaller ρ_1 (Figure 7(a)). We also find that systems with higher f reach lower ρ_2/ρ_1 towards merging (for q less than 0.10) and that the ratio ρ_2/ρ_1 of systems with the same mass ratio follows a downward trend as the fill-out factor f increases (Figure 7(b) and (c), respectively).

To investigate the dynamical stability of all nine systems with mass ratios that are extremely close to the minimum mass ratio for contact systems, we calculate the ratio of the spin angular momentum ($J_{\rm s}$) to the orbital angular momentum ($J_{\rm o}$) using the formula derived from Equations (1) and (2) of Li & Zhang (2006), namely

$$\frac{J_{\rm s}}{J_{\rm o}} = \frac{(1+q)}{q}(k_1 r_1)^2\left[1 + q\left(\frac{k_2}{k_1}\right)^2\left(\frac{r_2}{r_1}\right)^2\right], \qquad (2)$$

where k_1, k_2 are the dimensionless gyration radii of both components. As the value of k, which determines the interior structure of the star, is the primary source of uncertainty, we initially adopt $k_1^2 = k_2^2 = k^2 = 0.06$ (Sun-like) as in Rasio (1995). The ratio values $J_{\rm s}/J_{\rm o}$ for the nine LMR systems are all

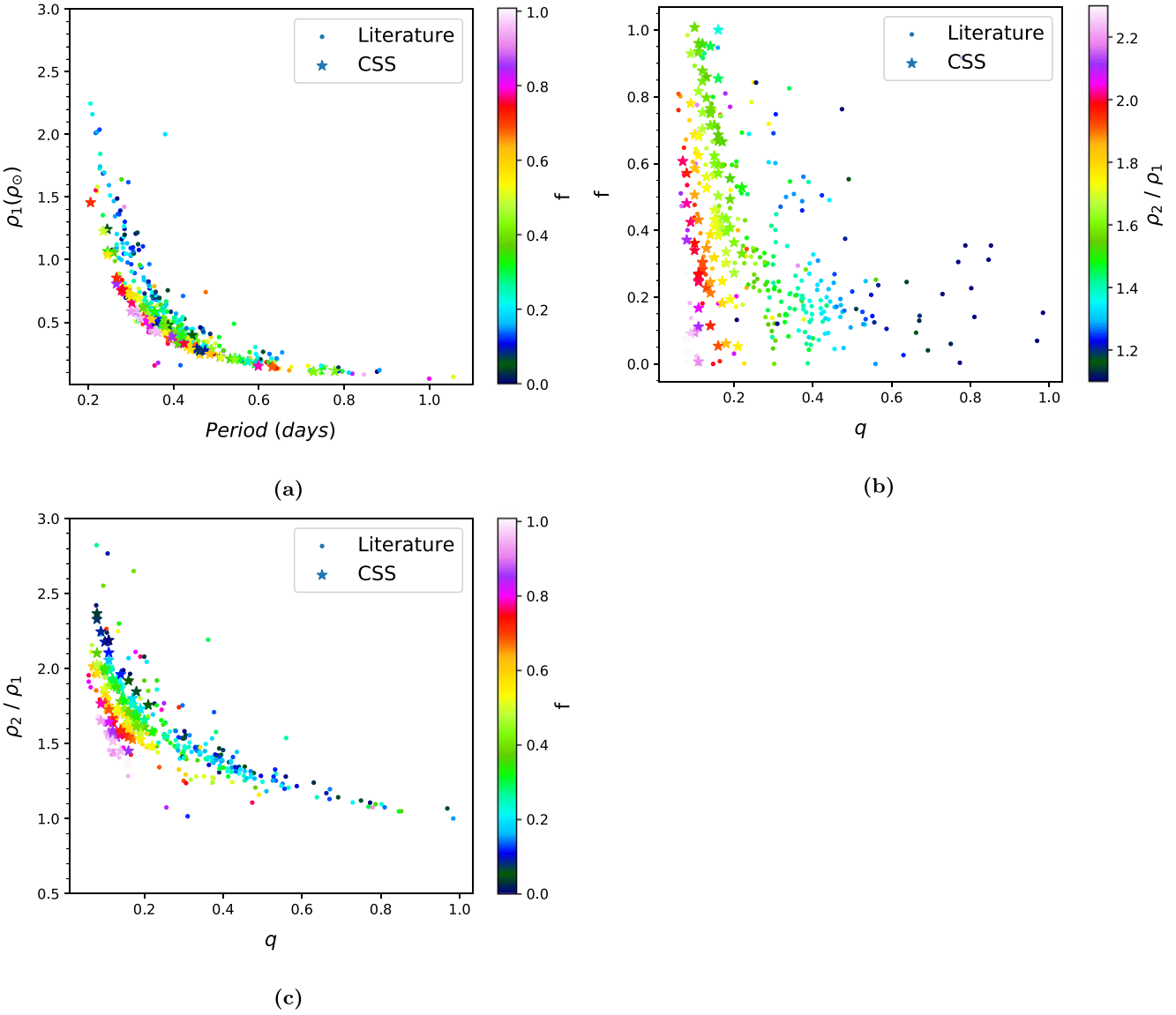

Figure 7. (a) The mean density of the primary component $\rho_1(\rho_\odot)$ as a function of period and fill-out factor f. (b) The mass ratio q as a function of fill-out factor f and the ratio of densities ρ_2/ρ_1. (c) The ratio of densities ρ_2/ρ_1 of the components as a function of mass ratio q and fill-out factor f. Color coded according to the scale on the right.

below 1/3, indicating that all systems are stable. The ratio was then adjusted using the value of $k_2^2 = 0.205$ (Arbutina 2007) for a convective secondary due to its very low mass. The value of k_1 was derived from the linear $k_1 - M$ relationships provided by Christopoulou et al. (2022), which are based on the values tabulated by Landin et al. (2009). Specifically, we use $k_1 = -0.250\,M + 0.539$ for stars with $M = 0.5$–$1.4\,M_\odot$, and $k_1 = 0.014\,M + 0.152$ for stars with $M > 1.4\,M_\odot$. There are only two systems with a $(J_s/J_o)_k$ ratio close to 1/3, J090748 (0.30) and J231513 (0.28). Nevertheless, for J231513 the ratio $(J_s/J_o)_k$ reduces to 0.24 when we use the results of the spotted solution from our VRI LCs. The nonuniqueness of the spotted solutions is an old issue in the modeling of contact binaries so there are potentially other solutions that may show that systems such as J231513 are stable. Another issue with spotted solutions is that the LCs of contact binaries at different passbands of the surveys (ASAS-SN, ZTF, TESS) and of the dedicated observations (Papageorgiou et al. 2023) do not always show the same asymmetry (variable O'Connell effect), and this may alter the geometric solution and subsequently the absolute parameters.

The degenerate solutions (different but equally well fitting spotted light-curve solutions) in the LC modeling, lead to the degeneracy of instability parameters such as the instability mass ratio q_{inst}, which depends on the mass of the primary component and the fill-out factor (Wadhwa et al. 2021) and/or the metallicity (Wadhwa et al. 2024). This highlights the need to find a different instability criterion in the absence of Doppler Imaging analysis and high dispersion spectra.

As interesting as the end of an LMR's life is, so are their ancestors. Even though many questions remain regarding the specific evolutionary process through the detached channel, the initial masses of the two components play a critical role in the evolution to the contact phase. Yildiz & Doğan (2013) proposed a scenario that allows us to calculate these values, based on the findings from the mass–luminosity and mass–radius diagrams. In this framework, primary components of EWs reside in the region

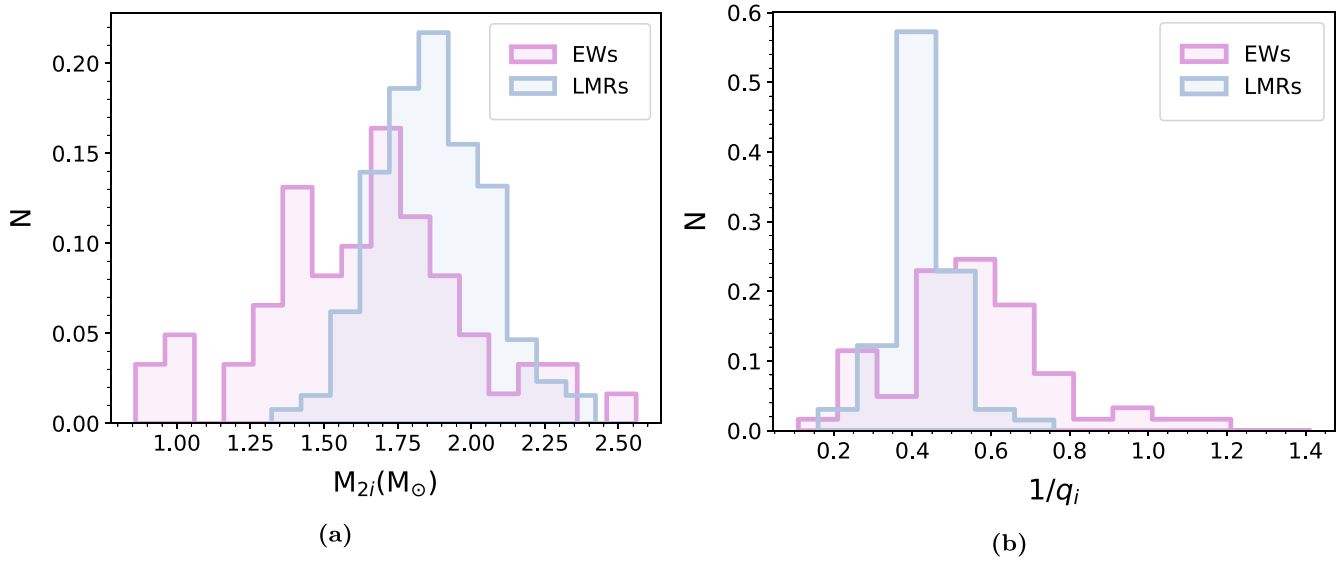

Figure 8. (a) The mass distribution of the progenitors of the initial massive component (M_{2i}) and (b) the distribution of the initial mass ratio ($1/q_i$) of the progenitors of LMRs from CSS and Yildiz & Doğan (2013) and EWs with $q > 0.25$ from the latter.

of unevolved low-mass single stars between the zero-age main sequence and terminal-age main sequence, while secondaries are systematically oversized and overluminous for their masses. Assuming a reversal of roles and mass transfer, with both components expanding beyond their Roche lobes and sharing a common envelope, following the above method, we calculated the initial mass of the primary (M_{1i}) and the secondary component (M_{2i}) as well as the initial mass ratio ($1/q_i$) for the 92 CSS LMRs. The results of the above procedure on the 92 CSS LMRs show that the mean mass of the progenitors is $M_{2i} = 1.87 \pm 0.21\,M_\odot$ and $M_{1i} = 0.78 \pm 0.16\,M_\odot$. As is shown in Figure 8(a), the distribution of the masses of the progenitors of the initial massive components (M_{2i}) of our LMRs and EW sample (62 spectroscopic studied EWs with $q > 0.25$; from Yildiz & Doğan 2013) reveals that LMR systems tend to originate from higher-mass ancestors. This could imply that, similarly to single stars, their evolution is mainly dictated by the thermonuclear reactions taking place in their cores. In the case of ultra-short-period EWs, on the other hand, evolution is instead primarily regulated by AML, mass loss, and magnetic braking (Papageorgiou et al. 2023).

In order to achieve our initial objective of applying the same technique for identification, photometric analysis, modeling, and extraction of absolute parameters to a homogeneous sample (CSS) of LMRs for further quantitative conclusions and discussion of mini statistics, it is important to clarify that we did not use data from TESS (where available). Future research on the most intriguing LMRs will involve a period variation study as well as TESS analysis together with multiband ZTF (gri), ASAS-SN light curves, and other surveys as in Papageorgiou et al. (2023).

Acknowledgments

E.L. gratefully acknowledges the support provided by IKY "Scholarship Programme for PhD candidates in the Greek Universities." A.P. gratefully acknowledges the support provided by the grant cofinanced by Greece and the European Union (European Social Fund; ESF) through the Operational Programme «Human Resources Development, Education and Lifelong Learning» in the context of the project "Reinforcement of Postdoctoral Researchers-2nd Cycle" (MIS-5033021), implemented by the State Scholarships Foundation (IKY). Support for C.E.F.L. and M.C. is provided by ANID's FONDECYT Regular grant 1231637 and Millennium Science Initiative grant ICN12_009, awarded by ANID to the Millennium Institute of Astrophysics (MAS). Additional support for M.C. is provided by ANID's Basal grant FB210003. This work is based on observations made with the 2.3 m Aristarchos telescope, Helmos Observatory, Greece, which is operated by the Institute for astronomy, astrophysics, space applications, and remote sensing of the National Observatory of Athens, Greece. The publication fees of this manuscript have been financed by the Research Council of the University of Patras.

Facilities: CSS

Software: PHOEBE-0.31A (Prša & Zwitter 2005), MWDUST (Bovy et al. 2016), PYRAF (Science Software Branch at STScI 2012), ASTROMETRY.NET (Lang et al. 2010).

Appendix
New LMR Candidates from ASAS-3

We apply the same method as described by Lalounta et al. (2020) and Christopoulou et al. (2022) on the eclipsing binary catalog of All Sky Automated Survey (ASAS-3, Pojmanski 1997, 2002) and identified 98 LMR candidates. Table 4 lists the reference time of minimum HJD_0, the Period (days), and the ASAS-3 magnitude V_{ASAS} (mag). Approximately 21 out of the 98 candidates are confirmed LMRs in previous studies (denoted by α in Table 4) are potential red nova progenitors according to Wadhwa et al. (2022; denoted by b in Table 4). Together, the 37 new LMRs from CSS and the 77 LMR candidates from ASAS-3 provide an excellent chance for ground-based dedicated observations to further whittle down the list of possible mergers.

Table 4
The 98 LMR Candidates from ASAS-3

Name	HJD_0 (2450000 +)	Period (days)	V_{ASAS} (mag)	Name	HJD_0 (2450000 +)	Period (days)	V_{ASAS} (mag)
ASAS _ J 001556+0644.7	3169.92649	0.4012003	11.17	ASAS _ J 101159+1652.5[a]	2667.77002	0.2667329	11.46
ASAS _ J 004717-1941.6	3185.86545	0.4888105	11.31	ASAS _ J 101818-5154.6	2634.81936	0.5846602	10.29
ASAS _ J 014255-2007.5	2460.98228	0.3659550	11.11	ASAS _ J 102556+2049.3	4476.83060	0.2849765	10.43
ASAS _ J 015937-0331.0	2644.55908	0.6315200	9.35	ASAS _ J 103231+1608.6	2689.73888	0.6456704	10.63
ASAS _ J 023152-3837.4	4400.65914	0.5887406	9.91	ASAS _ J 105210-4345.5	3403.80885	0.6104604	10.91
ASAS _ J 032629-3101.3	1876.61098	0.6386700	10.81	ASAS _ J 111131-0815.7	2740.63563	0.6008158	9.79
ASAS _ J 033142-5927.4	2921.83140	0.3779974	12.17	ASAS _ J 122119-1359.9[a]	1962.73746	0.4745019	10.98
ASAS _ J 034202-5145.2	3631.78155	0.4092128	10.82	ASAS _ J 124338-4656.1	2831.59247	0.6693620	10.23
ASAS _ J 034809-5839.8	3798.52851	0.4292427	10.48	ASAS _ J 125736+0749.2	2804.56497	0.3636122	11.61
ASAS _ J 035020-8017.4[a]	4553.49053	0.6224005	11.94	ASAS _ J130226+0718.6	3186.58347	0.4080725	11.70
ASAS _ J 035200-2155.8	2136.81948	0.3351662	10.69	ASAS _ J 135314+2009.7	3129.66797	0.5315500	10.34
ASAS _ J 040315+1411.5	2987.70073	0.3803151	11.79	ASAS _ J 143652-6646.6	3113.76872	0.7020080	10.44
ASAS _ J 040528-6536.2	3767.69194	0.2947729	11.91	ASAS _ J 144235-4027.2[a]	1996.73775	0.3250320	10.83
ASAS _ J 040550-5402.6	3792.74450	0.3601228	11.51	ASAS _ J 145538-7948.4[a]	1980.73633	1.0655580	9.13
ASAS _ J 041138-4438.0	3437.53380	0.8945652	9.42	ASAS _ J 153708-0606.3	2879.53968	0.9179296	10.67
ASAS _ J 045211-2511.7	3407.62308	0.5789031	11.41	ASAS _ J 155025-0757.3	3901.70901	0.3578460	11.72
ASAS _ J 045707-7207.9	2962.71682	0.4183947	12.08	ASAS _ J 160847+2511.7	4229.60604	0.3502237	11.60
ASAS _ J 050334-2521.9[a]	2197.76363	0.4140682	11.09	ASAS _ J 170715-5118.7[a]	2834.76161	0.5258890	11.40
ASAS _ J 051306+1558.2[a]	3266.86384	0.3830040	11.75	ASAS _ J 171905-6313.2	2068.65499	0.4547656	10.71
ASAS _ J 052650-8135.2	4216.46844	0.4616655	8.17	ASAS _ J 173400+1614.0	3273.58466	0.9736282	11.07
ASAS _ J 055624-5919.5	3653.81800	0.6191750	11.88	ASAS _ J 173638-6648.1	2502.57297	0.4419562	11.19
ASAS _ J055827-1739.8	3430.64794	0.4145902	10.15	ASAS _ J 175656-3055.3	4540.88949	0.3952890	11.67
ASAS _ J 060011-1549.8	4336.87729	0.4169109	12.02	ASAS _ J 180157-7228.1	4204.86185	0.3559101	10.48
ASAS _ J 061627-7426.8	3779.68621	0.6304502	10.63	ASAS _ J 180433-4213.4	3832.85690	0.7008844	8.22
ASAS _ J 061717-3427.6	3017.58607	0.5344865	11.02	ASAS _ J 181003-8126.2	4315.71549	0.3815023	11.56
ASAS _ J 061758-0714.2	3433.69821	1.1280524	9.40	ASAS _ J 183317-4208.7	2879.16287	0.4566467	11.59
ASAS _ J 061911-1548.3	3826.49788	0.4109543	10.47	ASAS _ J 184644-2736.4[a,b]	2863.48857	0.3028361	11.65
ASAS _ J 063420-4833.3	2258.70701	0.3215688	9.16	ASAS _ J 185354-3454.0	2795.77601	0.3946822	10.82
ASAS _ J 063546+1928.6[a]	4433.71624	0.4755129	9.95	ASAS _ J 190704+0742.0	2561.51030	0.8136180	10.76
ASAS _ J 065227-5524.6	2244.77458	0.7228700	11.14	ASAS _ J 191205-4013.7	2909.66317	0.6457323	11.79
ASAS _ J 065357-3648.1	3801.55019	0.3983703	10.84	ASAS _ J 192111-2228.9	4163.87647	0.8123023	11.49
ASAS _ J 065638-3850.1	2213.76269	0.4257200	10.36	ASAS _ J 192349+0818.4[a]	3467.88454	0.4237983	9.12
ASAS _ J 070140-1514.1	3363.68534	0.5885460	11.78	ASAS _ J 192626-3019.2	4400.57511	0.4469845	10.37
ASAS _ J 071451-5916.1[a]	3511.45194	0.4722930	9.17	ASAS _ J 193822-0332.6[a]	3159.75451	0.4127745	10.86
ASAS _ J 071603-3052.1	2755.53485	0.3699650	11.26	ASAS _ J 194512-1932.8	3851.89999	0.6728200	10.92
ASAS _ J 072525+1052.1	3795.65301	0.5401389	11.28	ASAS _ J 194625+0845.1[a]	2861.61954	0.4175379	11.41
ASAS _ J 073246-2047.5[a]	1876.69086	0.8192500	8.40	ASAS _ J 200304-0256.0[b]	2902.52596	0.4571957	10.60
ASAS _ J 073516-4842.9	3462.58991	0.4310640	11.80	ASAS _ J 201125-0632.0	2144.61137	1.1884401	10.13
ASAS _ J 075125+0454.6	3820.54204	0.7928613	10.16	ASAS _ J 201934-2726.8	4191.07671	0.4074481	12.32
ASAS _ J 082205-6556.3	2618.71516	0.7419419	9.55	ASAS _ J 203141-5353.4	3705.55492	0.3519324	10.84
ASAS _ J 082243+1927.0[a,b]	3410.65967	0.2800459	11.26	ASAS _ J 203445-7237.0	4333.63344	0.4077932	10.61
ASAS _ J 082704+0330.9[a]	2977.79834	0.3278289	9.95	ASAS _ J 204625-1247.1	3554.77871	0.4275123	11.05
ASAS _ J 083226-2910.1	2899.87530	0.6878800	10.56	ASAS _ J 204628-7157.0[a]	3444.90678	0.7950000	8.62
ASAS _ J 085335-7028.1	2619.75101	0.6389400	10.60	ASAS _ J 211902-0842.4	3581.81767	1.1746938	10.90
ASAS _ J 091010+0344.6[a]	3030.75836	0.4722758	11.09	ASAS _ J 212146-6544.2	4245.87043	0.6556112	9.66
ASAS _ J 093547-1335.2	3672.87506	0.3510754	9.93	ASAS _ J 213209-3442.9	4295.83307	0.3766000	10.20
ASAS _ J 093818-6755.4	3411.68022	0.3898983	10.26	ASAS _ J 214322+1442.5	3596.74982	0.5770898	11.27
ASAS _ J 093838-5749.4	1977.58848	0.4382420	10.94	ASAS _ J 215035-2748.6[a,b]	2974.53368	0.3738857	9.29
ASAS _ J 100524-1416.3	2248.75486	0.4416701	11.51	ASAS _ J 215711+2240.2	3330.51545	0.4220225	9.56

Notes.
[a] Systems that have already been studied. All of them are confirmed LMRs.
[b] LMR systems included in the catalog of Wadhwa et al. (2022) that are potential red nova progenitors.

ORCID iDs

Athanasios Papageorgiou https://orcid.org/0000-0002-3039-9257
Márcio Catelan https://orcid.org/0000-0001-6003-8877

References

Akerlof, C., Amrose, S., Balsano, R., et al. 2000, AJ, 119, 1901
Arbutina, B. 2007, MNRAS, 377, 1635
Arbutina, B. 2009, PASP, 121, 1036
Bellm, E. C., Kulkarni, S. R., Graham, M. J., et al. 2019, PASP, 131, 018002
Bovy, J., Rix, H.-W., Green, G. M., Schlafly, E. F., & Finkbeiner, D. P. 2016, ApJ, 818, 130
Butters, O. W., West, R. G., Anderson, D. R., et al. 2010, A&A, 520, L10
Christopoulou, P.-E., Lalounta, E., Papageorgiou, A., et al. 2022, MNRAS, 512, 1244
Cui, X.-Q., Zhao, Y.-H., Chu, Y.-Q., et al. 2012, RAA, 12, 1197
Darwin, G. H. 1879, Proc. R. Soc. (London) A, 29, 168, http://www.jstor.org/stable/113751

Devarapalli, S. P., Jagirdar, R., Prasad, R. M., et al. 2020, MNRAS, 493, 1565
Drake, A. J., Catelan, M., Djorgovski, S. G., et al. 2013, ApJ, 763, 32
Drake, A. J., Djorgovski, S. G., Mahabal, A., et al. 2009, ApJ, 696, 870
Drake, A. J., Gänsicke, B. T., Djorgovski, S. G., et al. 2014b, MNRAS, 441, 1186
Drake, A. J., Graham, M. J., Djorgovski, S. G., et al. 2014a, ApJS, 213, 9
Gaia Collaboration, Vallenari, A., & Brown, A. G. A. 2023, A&A, 674, A1
Green, G. M., Schlafly, E., Zucker, C., Speagle, J. S., & Finkbeiner, D. 2019, ApJ, 887, 93
Hambálek, Ľ., & Pribulla, T. 2013, CoSka, 43, 27
Heinze, A. N., Tonry, J. L., Denneau, L., et al. 2018, AJ, 156, 241
Hut, P. 1980, A&A, 92, 167
Kochanek, C. S., Adams, S. M., & Belczynski, K. 2014, MNRAS, 443, 1319
Lalounta, E., Papageorgiou, A., Christopoulou, P. E., & Catelan, M. 2020, CoSka, 50, 409
Landin, N. R., Mendes, L. T. S., & Vaz, L. P. R. 2009, A&A, 494, 209
Lang, D., Hogg, D. W., Mierle, K., Blanton, M., & Roweis, S. 2010, AJ, 139, 1782
Latković, O., & Čeki, A. 2021, PASJ, 73, 132
Latković, O., Čeki, A., & Lazarević, S. 2021, ApJS, 254, 10
Li, L., & Zhang, F. 2006, MNRAS, 369, 2001
Liu, F., Li, K., Gao, X., et al. 2024, MNRAS, 527, 6406
Liu, X.-Y., Li, K., Michel, R., et al. 2023, MNRAS, 519, 5760
Lucy, L. B. 1967, ZAp, 65, 89
Nandez, J. L. A., Ivanova, N., & Lombardi, J. C. J. 2014, ApJ, 786, 39
O'Connell, D. J. K. 1951, MNRAS, 111, 642
Papageorgiou, A. 2015, PhD thesis, University of Patras
Papageorgiou, A., Catelan, M., Christopoulou, P.-E., Drake, A. J., & Djorgovski, S. G. 2018, ApJS, 238, 4
Papageorgiou, A., Catelan, M., Christopoulou, P.-E., Drake, A. J., & Djorgovski, S. G. 2019, ApJS, 242, 6
Papageorgiou, A., & Christopoulou, P. E. 2015a, in ASP Conf. Ser. 496, Living Together: Planets, Host Stars and Binaries, ed. S. M. Rucinski, G. Torres, & M. Zejda (San Francisco, CA: ASP), 181
Papageorgiou, A., & Christopoulou, P. E. 2015b, AJ, 149, 168
Papageorgiou, A., Christopoulou, P.-E., Ferreira Lopes, C. E., et al. 2023, AJ, 165, 80
Pecaut, M. J., & Mamajek, E. E. 2013, ApJS, 208, 9
Pojmanski, G. 1997, AcA, 47, 467
Pojmanski, G. 2002, AcA, 52, 397
Prša, A. 2018, Modeling and Analysis of Eclipsing Binary Stars (Bristol: IOP Publishing)
Prša, A., & Zwitter, T. 2005, ApJ, 628, 426
Qian, S.-B., Zhu, L.-Y., Liu, L., et al. 2020, RAA, 20, 163
Rasio, F. A. 1995, ApJL, 444, L41
Ruciński, S. M. 1973, AcA, 23, 79
Science Software Branch at STScI 2012, PyRAF: Python alternative for IRAF, Astrophysics Source Code Library, ascl:1207.011
Şenavcı, H. V., Doğruel, M. B., Nelson, R. H., Yılmaz, M., & Selam, S. O. 2016, PASA, 33, e043
Stassun, K. G., Oelkers, R. J., Paegert, M., et al. 2019, AJ, 158, 138
Stępień, K. 2011, A&A, 531, A18
Sun, W., Chen, X., Deng, L., & de Grijs, R. 2020, ApJS, 247, 50
Terrell, D., & Wilson, R. E. 2005, Ap&SS, 296, 221
Tylenda, R., Hajduk, M., Kamiński, T., et al. 2011, A&A, 528, A114
van Hamme, W. 1993, AJ, 106, 2096
Wadhwa, S. S., De Horta, A., Filipović, M. D., et al. 2021, MNRAS, 501, 229
Wadhwa, S. S., De Horta, A. Y., Filipović, M. D., et al. 2022, JApA, 43, 94
Wadhwa, S. S., DeHorta, A. Y., Filipović, M., & Tothill, N. F. H. 2023, AN, 344, e20220066
Wadhwa, S. S., Landin, N. R., Kostić, P., et al. 2024, MNRAS, 527, 1
Yildiz, M., & Doğan, T. 2013, MNRAS, 430, 2029
Zheng, S.-Y., Li, K., & Xia, Q.-Q. 2021, MNRAS, 506, 4251
Zwitter, T., Munari, U., Marrese, P. M., et al. 2003, A&A, 404, 333